

## CHAPTER 8

---

---

# Detection of Fires and Power Outages Using DMSP-OLS Data

---

---

Christopher D. Elvidge, Kimberly E. Baugh, Vinita Ruth Hobson,  
Eric A. Kihn, and Herbert W. Kroehl

### 1.0 INTRODUCTION

Recently developed algorithms for processing nighttime data acquired by the Defense Meteorological Satellite Program (DMSP) Operational Linescan System (OLS) make it possible to detect fires and power outages worldwide. The DMSP-OLS has a unique capability to observe faint sources of visible-near infrared emissions present at night on the Earth's surface (Figure 8.1), including cities, towns, villages, gas flares, and fires (Croft 1973, 1978, 1979). By analyzing a time series of DMSP-OLS images, it is possible to define a reference set of "stable" lights that are present in the same location on a consistent basis. Fires are identified as lights detected on the land surface outside the reference set of stable lights. Power outages are detected based on the absence of lights in locations within the reference set of stable lights.

Since the early 1970s the U.S. Air Force has operated DMSP polar orbiting platforms carrying cloud imaging satellite sensors capable of detecting clouds using two broad spectral bands: visible-near infrared (visible-near infrared) and thermal infrared (TIR). The program began with the SAP (Sensor Aerospace Vehicle Electronics Package) which were flown from 1970–1976. The current generation of OLS sensors began flying in 1976 and are expected to continue flying until ~2010. At night the visible band is intensified with a photomultiplier tube to permit detection of clouds illuminated by moonlight. While DMSP data were not officially classified, digital data were not available or preserved during the first 20 years of the program. An OLS film archive at the University of Colorado, National Snow and Ice Data Center provided the scientific community with access to a subset of OLS data in analog form. A digital archive for the DMSP-OLS data was established in mid-1992 at the NOAA National Geophysical Data Center.

The potential use of DMSP-OLS data for the inventory of human settlements and energy consumption patterns has been noted since the 1980s (Welch, 1980; Foster, 1983). Sullivan (1989) produced a 10 km resolution global image of OLS-observed visible-near infrared emission sources using film data. These early studies with OLS data relied on the analysis of film strips, which limited the studies on population and energy to a small number of sites. The first global map of nighttime lights observed with DMSP-OLS data, published by Sullivan (1989), was also derived from film, selected based on the presence of large number cloud-free visible-near infrared emission sources and mosaicked into a global product. As a result, many of the features presented in areas such as Africa are ephemeral visible-near infrared emissions from

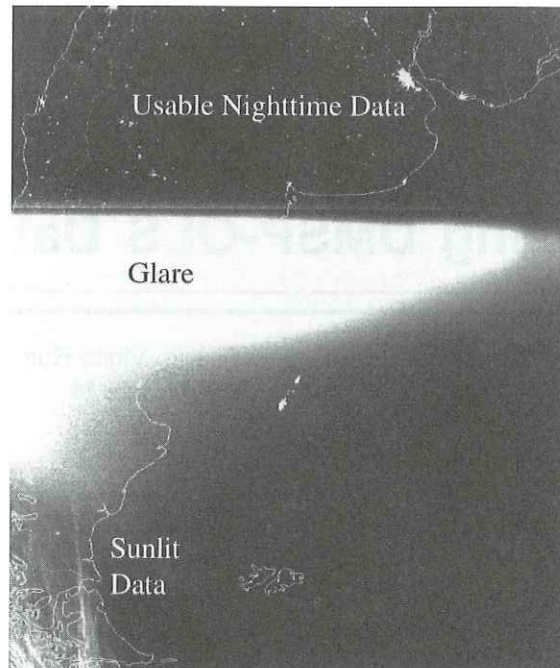


**Figure 8.1.** Nighttime visible band DMSP-OLS data of Chile and Argentina acquired January 27, 1995 showing city lights, sunlight contamination and solar glare.

fires. The only systematic use of film data for the analysis of fires was the inventory of African fires reported by Cahoon et al. (1992).

Recent results obtained at NOAA-NGDC with the digital DMSP-OLS data (Elvidge et al., 1996 and 1997) suggest that nightly broad area inventories of fires and power outages could be readily produced. Algorithms have been developed to identify and geolocate visible-near infrared emission sources in nighttime OLS imagery. This chapter describes the procedures which have been developed for detection of ephemeral events (fires and power outages) in DMSP-OLS data. The method relies on identifying a reference set of stable lights (cities, towns, villages, gas flares) database using a time series of OLS observations. Once the stable lights data set has been derived, it is possible to overlay the lights from an individual orbit to detect new visible-near infrared emission sources (e.g., fires) or locations where visible-near infrared emission was expected, but not observed (power outages).

## 2.0 THE DMSP OPERATIONAL LINESCAN SYSTEM

The DMSP generally operates two satellites in sun-synchronous orbits, one in a dawn-dusk orbit, the other in a day-night orbit. The Operational Linescan System (OLS) is an oscillating scan radiometer designed for cloud imaging with two spectral bands (visible and TIR) and a swath of ~3000 km. The “visible” bandpass straddles the visible and near-infrared (visible-near infrared) portion of the spectrum (0.5 to 0.9  $\mu\text{m}$ ). Satellite attitude is stabilized using four gyroscopes (three axis stabilization), a star mapper, Earth limb sensor, and a solar detector. The OLS visible band signal is intensified at night using a photomultiplier tube (PMT), for the detection of moonlit clouds (Figure 8.1). The low light sensing capabilities of the OLS at night

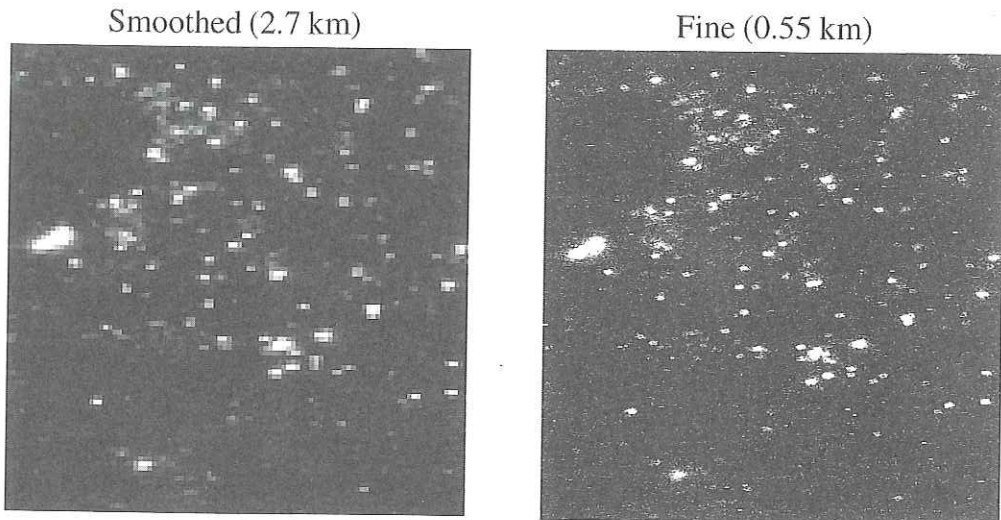


**Figure 8.2.** Simultaneously acquired smoothed versus fine resolution nighttime visible band DMSP-OLS of fires in Para, Brazil.

permit the measurement of radiances down to  $10^{-9}$  watts/cm<sup>2</sup>/sr/μm. This is more than four orders of magnitude lower than the OLS daytime visible band or the visible-near infrared bands of other sensors, such as the NOAA AVHRR or the Landsat Thematic Mapper.

There are two spatial resolution modes in which OLS data can be acquired. The full resolution data, having nominal spatial resolution of 0.56 km, is referred to as "fine." Onboard averaging of five by five blocks of fine data produces "smoothed" data with a nominal spatial resolution of 2.7 km. Most of the data received by NOAA-NGDC is in the smoothed spatial resolution mode. Acquisitions of the fine resolution data can be made (on a noninterference basis) through request to the Air Force. There are spatial details present in the fine resolution data that are absent in the smoothed data. Figure 8.2 shows examples of smoothed versus fine resolution nighttime visible band data of fires in the state of Para, Brazil on August 22, 1995.

The OLS uses several methods to constrain the enlargement of pixel dimensions which normally occur as a result of cross track scanning (Lieske, 1981). The OLS features a sinusoidal scan motion, which maintains a nearly constant along track pixel-to-pixel ground sampling distance (GSD) of 0.56 km at all scan angles in the fine resolution data. The along scan GSD for fine resolution data starts at 0.31 km at nadir and slowly rises to 0.55 km at 1200 km surface distance from nadir, decreasing again to 0.5 km by the end of scan. The detector image rotates as a function of the scan angle and the shape, size, and orientation of the OLS detectors were designed to take advantage of this rotation to reduce the expansion of the EIFOV (effective instantaneous field of view) at off-nadir scan angles. In addition, the PMT electron aperture is magnetically switched (deflected) during the outer quarter of each scan, again reducing the size of the detector image on the ground surface. The EIFOV of the nighttime visible band fine resolution data starts at 2.2 km at the nadir and expands to 4.3 km at 766 km out from the nadir. After the aperture is switched, the IFOV is reduced to 3.0 km and expands to 5.4 km at the far edges of the scan. Thus the EIFOV is substantially larger than the GSD in both the along track and along scan directions.

The gain for the OLS is programmed to track changes in illumination associated with the lunar cycle. The lowest gain setting coincide with the full moon, at which time clouds and the

outline of land surface features such as coastlines and major drainage patterns can be readily observed in visible band data. High visible band gain settings are used during the darkest 10–12 nights of each lunar cycle, when lunar illumination at the time of the DMSP overpass is less than half of the maximum possible. Even with the high gain settings, clouds and most of the earth's surface remain dark in OLS data acquired during the darkest nights of the lunar cycle, leaving visible-near infrared emission sources as the primary features observable in the nighttime visible band data. As a result, fainter areas of visible-near infrared emission are detectable in OLS data acquired under new moon conditions than under full moon conditions.

### **3.0 METHODS AND RESULTS**

#### **3.1 Stable Lights**

The procedures used to assemble stable lights databases are outlined in Figure 8.3. As an example, we will follow the steps used to generate a stable lights product of South America. The structure of the OLS data includes a byte for data quality which is used to tag pixels based on the presence or absence of a visible-near infrared emission source, cloud, or data quality problem. These tags are subsequently used in the time series analysis.

##### ***Scene Selection***

DMSP-OLS data from 246 smoothed resolution orbits of South America acquired with less than half lunar illumination conditions between October 27, 1994 and April 30, 1995 were extracted from the digital archive. We use data acquired with less than 50 percent lunar illumination for two reasons: (1) During these nights the visible-near infrared band gain on the OLS is set to its highest monthly level, permitting detection of smaller light sources present on the Earth's surface. And (2) With low levels of lunar illumination it is possible to avoid inclusion of moonlight reflectance off clouds and water, which can be confused with visible-near infrared emissions from anthropogenic activity.

##### ***Establishment of a Reference Grid***

We have used the one-kilometer grid developed for the NASA-USGS Global 1 km AVHRR project (Eidenshink and Faundeen, 1995) interrupted Goode Homolosine Projection (Goode, 1925; Steinwand, 1993). This projection is optimized to provide a uniform grid cell size at all latitudes and contiguous land masses (except Antarctica).

For South America, a 7700 line by 5300 sample reference grid of 1 km pixels was extracted from the global reference grid established for the 1 km AVHRR project (Eidenshink and Faundeen, 1995). Our reference grid begins (northwest corner) with line 10900, sample 7200 of the larger global grid. To fill geolocated OLS data into the reference grid we find the grid cell closest to the latitude and longitude of the OLS pixel center and fill in the surrounding three by three block of pixels.

##### ***Geolocation***

Our geolocation algorithm operates in the forward mode, projecting the center point of each pixel onto the Earth's surface. The geolocation algorithm estimates the latitude and longitude

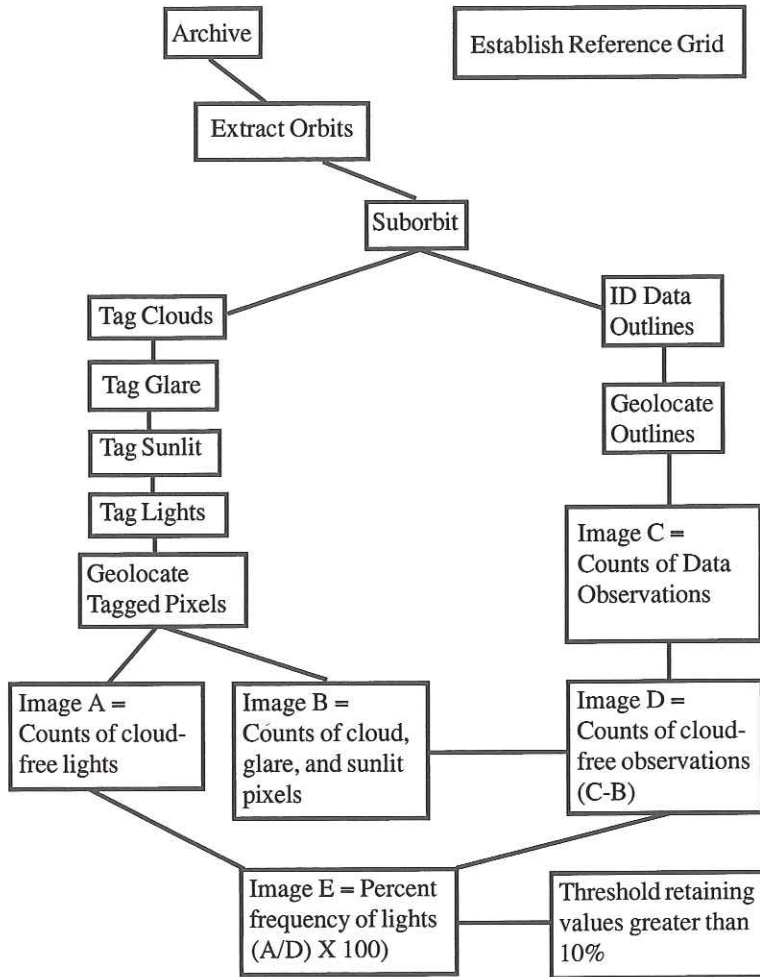


**Figure 8.3.** Flow chart indicating sequence of steps used to derive the nighttime lights from a time series of DMSP-OLS orbits.

of pixel centers based on the geodetic subtrack of the satellite orbit, satellite altitude, OLS scan angle equations, an Earth sea level model, and digital terrain data. The geodetic subtrack of each orbit is modeled using daily radar bevel vector sightings of the satellite (provided by Naval Space Command) as input into an Air Force orbital mechanics model that calculates the satellite position every 0.4208 seconds. The satellite heading is estimated by computing the tangent to the orbital subtrack. We have used an oblate ellipsoid model of sea level and have used Terrain Base (Row and Hastings, 1995) as a source of digital terrain elevations.

### **Tracking of Orbital Coverages**

The number OLS data coverages for each of the 1 km cells in the reference grid was determined by geolocating the outer perimeters of the OLS data segments from each orbit to create coverage polygons. Areas inside the polygons were assigned values of 1. The total number of coverages for each grid cell can then be determined by adding the values of all the coverage

polygons in the time series (Figure 8.4). Total number of coverages over the majority of the continent range from 70 to 100.

### ***Glare and Sunlit Data Removal***

Data of southern portions of the continent were contaminated by sunlight (Figure 8.1) during dates near the southern hemisphere's summer solstice (December 21). Data was screened for sunlight contamination based on solar elevations reported for the nadir of each scanline. Pixels in scanlines with solar elevations exceeding 14 degrees were tagged as sunlit.

One adverse effect of the light intensification is that the OLS is quite sensitive to scattered sunlight. Under certain geometric conditions, portions of the OLS are illuminated by sunlight. Scattering of sunlight into the optical path results in visible band detector saturation (Figure 8.1), a condition referred to as glare. The exact shape and orbital position of the glare changes through the year. An automated algorithm has been developed to detect and remove glare from OLS images. The algorithm searches the OLS data to detect the occurrence of 100+ adjacent pixels of saturated data (DN=63). Once such a block of data is encountered, all adjacent pixels having DN values greater than 40 are tagged as glare.

### ***Cloud Screening***

Because of the low level of lunar illumination present in the suborbits, it was not possible to use the visible band to assist in the identification of clouds. The cloud screening was based entirely on thresholds set on the TIR band. Clouds are generally colder than the earth's surface. However, the separation of cloud pixels from earth surface pixels using TIR thresholding is complicated by seasonal, latitudinal, and altitudinal variations in the background earth surface temperature. The separation of clouds from earth surface pixels is relatively easy at low latitudes where there is generally a large temperature difference between pixels of cloud tops and pixels containing land or ocean. Because of the strong latitudinal effects on the TIR threshold for cloud screening in our data, we segmented each of the orbital sections into a series of latitudinal bands for determination of a TIR threshold for discrimination and tagging of the cloud pixels.

### ***Cloud Free Observation***

Cloud, glare, and sunlit pixels were geolocated and the pixels were projected into the reference grid, where a counter tallied the number of times each grid cell contained unusable data. The resulting image of cloud, glare, and sunlit pixel counts is subtracted from the counts of data observations (Figure 8.4), yielding an image of the cloud-free observations of the earth's surface (Figure 8.5). The vast majority of the land areas had more than 25 cloud-free observations. The lowest numbers of cloud-free observations occurred in the Amazon basin and in high elevation areas in the Andes mountains, where snow pack was probably misidentified as cloud cover in the OLS TIR band data.

### ***Identification of Visible-Near Infrared Emission Sources***

Because of brightness variations which occur within and between orbits, it is not possible to set a single digital number (DN) threshold for identifying visible-near infrared emission sources.

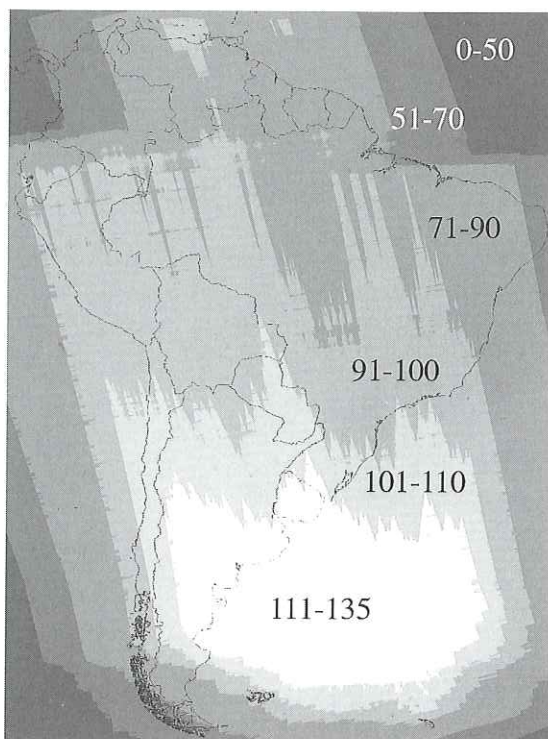


**Figure 8.4.** Number of nighttime OLS data coverages in the reference grid of the South America.

We have developed an algorithm for automatic detection of visible-near infrared emission sources (lights) in nighttime OLS data using thresholds established based on the local background. Lights are identified in 20 by 20 pixel blocks, with the local background being drawn from the surrounding 50 by 50 pixel block. This “light picking” algorithm excludes bright pixels in the selection of a background pixel set, which is then analyzed to establish a brightness threshold for the detection of visible-near infrared emission sources. The resulting threshold is applied to the central 20 by 20 pixel block inside the 50 by 50 pixel block. Processing of an image proceeds by tiling the results from adjacent 20 by 20 pixel blocks. Only pixels that were not previously tagged as cloud, glare, or sunlit are permitted to be tagged as visible-near infrared emission sources.

If an OLS line scan tracks across a cloud illuminated by lightning, a linear feature is produced which can be detected using the light picking algorithm described above. Typically the lighting is observed in one or two scan lines, but can occur in up to three or four scanlines if multiple lightning strikes continue to illuminate the same cloud mass. Because lightning is typically only detected in areas detected as cloud in the thermal band, the detects are generally excluded from the time series of observations used to generate the stable lights.

### **Identification of Stable Lights**

Pixels tagged as visible-near infrared emission sources are geolocated and projected into the reference grid, where a counter tallied the number of times each grid cell contained a light source. The image of light counts is then divided by the number of cloud-free observations

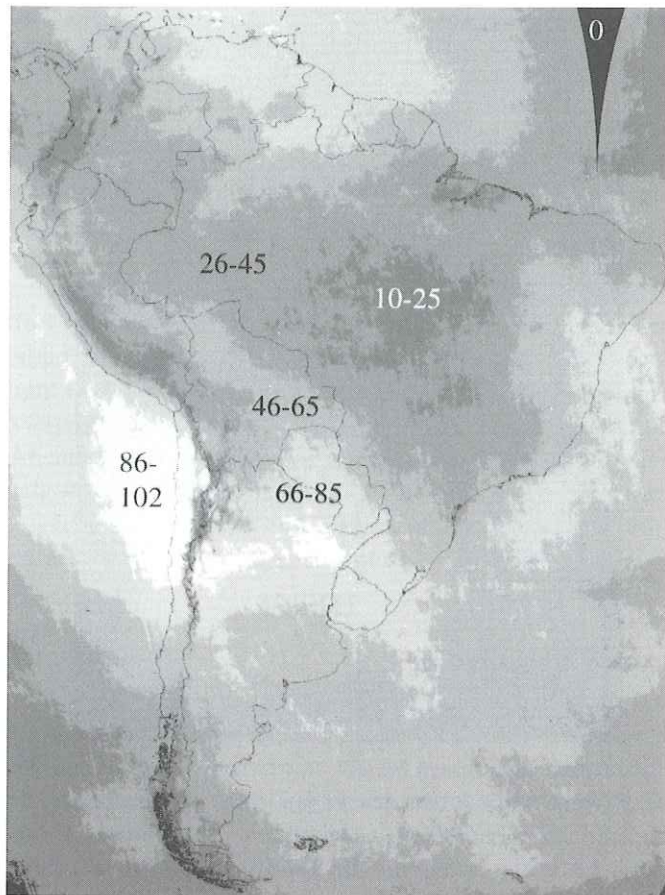


**Figure 8.5.** Number of cloud-free OLS data observations in the reference grid of South America.

(Figure 8.5) and the resulting real numbers are multiplied by 100 and truncated to byte values ranging from 0 to 100. These values represent the percent frequency with which visible-near infrared emission was detected in each grid cell based solely on cloud-free OLS observations. The locations of stable lights are defined as all areas which had DMSP-OLS detectable lights in at least 10 percent of the cloud-free observations. This 10 percent threshold was used to remove ephemeral visible-near infrared emission sources (fires, lightning, and random noise). In other regions of the world we were able to use a threshold of 6 percent, but random noise levels are higher over the region due to ionospheric disturbances over southern Brazil. The resulting georeferenced stable lights image of South America is shown in Figure 8.6. Larger cities were detected in 90 to 100 percent of the cloud-free observations. Smaller towns were detected with less frequency, in some cases only 10–20 percent of the time.

### 3.2 Identification of Fires

Fires are identified as visible band emission sources that are not associated with either stable lights or lightning. The procedure begins with the detection of lights and clouds in

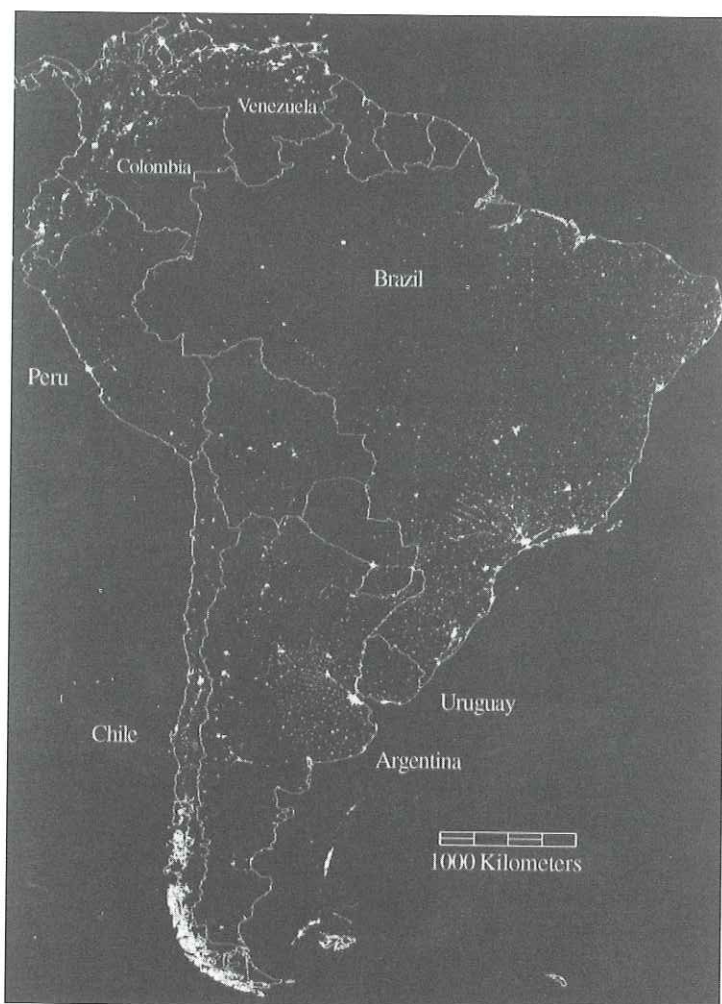


**Figure 8.6.** Nighttime lights of South America derived from cloud-free portions of 246 DMSP-OLS orbits acquired between October 1, 1994 and March 30, 1995.

incoming nighttime OLS using the algorithms described above. However, in the case of fire detection, lights detected in the presence of clouds are retained. In suborbits where visual inspection identifies the presence of lighting, the lightning illuminated pixels are manually removed. Lights and clouds are then geolocated and projected into the reference grid. Stable lights are then masked out with an algorithm that identifies all lit pixels which occur in or directly adjacent to the known stable light locations and sets their DN values to zero. The remaining pixels, which contain ephemeral visible band emission sources are taken to be fires. Figure 8.7 shows the fires which were detected from the September 8, 1996 nighttime OLS orbit over Brazil, during the peak of the burn season. By compositing burn observations from adjacent orbits over specific time intervals it is possible to assemble continental-scale depictions of the spatial and temporal patterns of biomass burning. Figure 8.8 shows the cumulative burn observed during a six month period over northern hemisphere Africa.

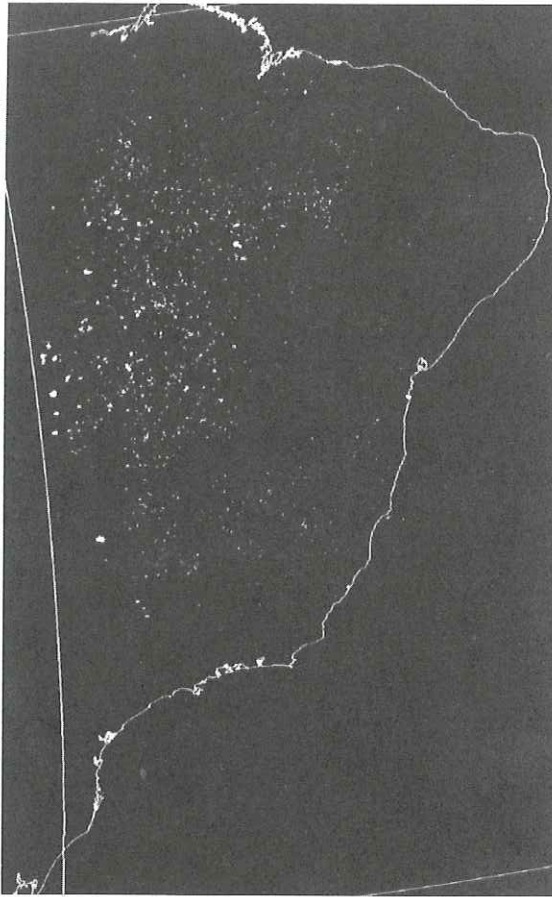


**Figure 8.7.** Nighttime fires in Brazil observed in a single DMSP-OLS orbit acquired September 8, 1996.

### 3.3 Identification of Power Outages

During the past 100 years electric power has become the principal source of nocturnal lighting in human settlements, roads, and industrial sites. Typically, electric production is centralized and the power is transmitted using a network of power lines and distribution wiring. Because many of the power lines and wires are aboveground, they are susceptible to damage, especially during severe weather events such as hurricanes, typhoons, thunderstorms, and in some instances snow or ice storms. Less frequent events, such as earthquakes, can also produce electric power outages. Another class of electric power outages, termed brownouts, results from an insufficient capacity to generate electric power or an inability to sustain the generation of electric power. In this case, the electric power supply becomes intermittent or is delivered at reduced levels.

Reporting on power outages is typically limited to eyewitness reports of individuals within the outage area. Because many types of communication (radio, television, telephone, facsimile) are also impacted by power outages, information on the extent of power outages during a disaster may be very incomplete. Having an observational basis for delineating the extent of power outages could provide valuable information to guide relief, repair, and cleanup efforts.

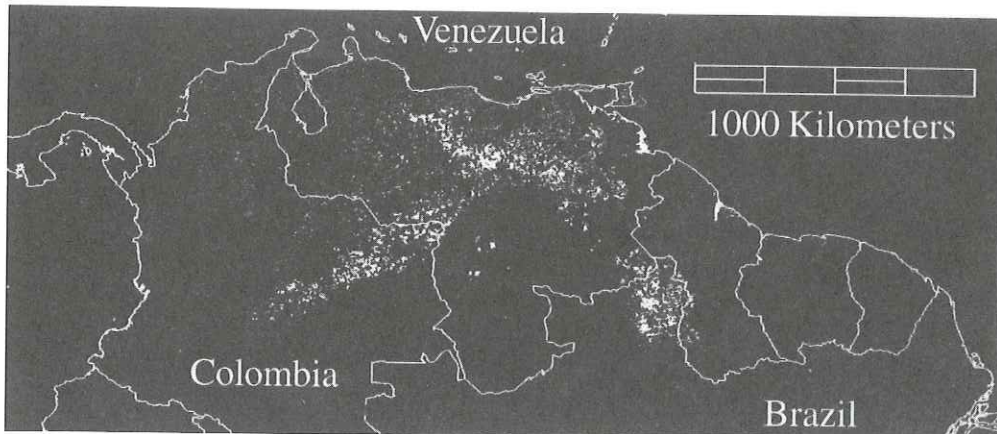


**Figure 8.8.** Cumulative DMSP-OLS fire detects in northern hemisphere Africa, October 1, 1994 through March 31, 1995.

Power outages are detected in nighttime DMSP-OLS data based on the absence of visible-near infrared emission in locations within the reference set of stable lights. As an example we present color Plate 15, which shows power outages detected September 7, 1996 in North Carolina following the September 6 passage of Hurricane Fran. The procedure for locating the power outages begins by overlying the lights detected on September 7 on top of the reference set of stable lights to form a color composite image. Because the September 7 nighttime OLS image was cloud-free, it was possible to examine the color composite and visually identify areas where power appeared to be on, areas with complete power outage, and areas that appeared to have partial power. Locations with power outage or partial power were manually outlined on the color composite. This outline was used to rearrange the color composite to generate the derived product shown in Plate 15. In areas where no power outage was detected, the reference set of stable lights are shown as white (Plate 15). In the outlined area containing power outages, detected visible-near infrared emissions are shown as white and power outage areas are shown as red. Thus towns shown as red had no power detected on September 7 and towns with partial power have a set of white pixels surrounded by red. For reference, the yellow line indicates the track of the hurricane center, as recorded by the National Hurricane Center. Note that most of the power outages occurred to the north of the hurricane landfall, encompassing the barrier islands of the central North Carolina coast. This is consistent with the fact that much of a hurricane's force, prior to landfall, is concentrated in its northeast quadrant. Moving inland, the zone of power outages tapers toward the overland track of the hurricane center. The OLS detected a diagonal corridor through the center of Raleigh, North Carolina where the power was knocked back harder than to either side. This corridor is parallel and adjacent to the hurricane path.

### 3.4 Factors Affecting the Detection of Fires and Power Outages

There are a number of factors or conditions which will impede the detection of fires and power outages with DMSP-OLS data, including: the OLS gain setting, cloud cover, and solar glare. The reference set of stable lights are derived using OLS data acquired during the darkest half of the lunar cycle, during which time the OLS visible band gain is set to its highest monthly

levels. During the full moon, the OLS visible band gain is set at a much lower state. As a result, many of the small towns indicated in the reference set of stable lights will not be detected in OLS data acquired during the full moon. Thus the detection of both power outages and fires with OLS data works best during the dark half of each lunar cycle. Fewer fires will be detected during the brightest nights of lunar illumination cycle. Without factoring in the gain changes, it would not be possible to distinguish power outages from detection losses associated with lower gain settings during the brightest nights of the month.

Heavy cloud cover blocks the transmission of visible-near infrared light from the earth's surface, blocking the observation of fires and power outages. Light cloud cover tends to diffuse lights present on the Earth's surface, making them appear larger than their actual size. Many fires are detected under light cloud cover; however, their outlines appear diffused. The diffusion caused by light cloud cover could cause partial power outages to be indistinguishable from the normal power conditions.

Other factors impeding the detection of fires and power outages include data dropouts, sunlight, and solar glare. Data dropouts occur randomly. Thus there is always some chance that DMSP-OLS data of a particular event will not be transmitted to NGDC. Solar glare results in unusable nighttime visible band data. This phenomenon precesses, and thus will affect portions of an orbit and gradually shift to the north or south. In some cases it is possible to use data from the edge of scan in an adjacent orbit to observe visible-near infrared emissions that are blocked by solar glare in the orbit. Sunlight will impact the detection of fires and power outages at high latitudes at or near the summer solstice.

The digital values in the reference set of stable lights indicate the percent frequency with which the light was detected in the set of cloud-free OLS observations. If a light source is reported to occur in 93 percent of the cloud-free observations and it is missing, along with a large number of its neighbors on a night following a natural disaster, then there is little doubt that the power is out. For small towns that are near the detection limits of the OLS, which may be detected in 15–20 percent of the cloud-free observations, the interpretation of the results gets trickier. Here again, the interpretation must rely on the local pattern of visible-near infrared emission detects. For instance, if town "A" has a detection frequency of 17 percent and no emission detected on a particular night and is surrounded by power outages in neighboring towns with higher detection frequencies, while nearby towns with detection frequencies in the 15–20 percent range had emissions the same night, then it would be reasonable to conclude that there is a high probability that town "A" has a power outage along with its neighbors.

#### 4.0 SUMMARY

We have outlined the algorithms for nighttime fire and power outage detection with data from the DMSP-OLS and provided examples. While other sensors, such as GOES and NOAA-AVHRR have demonstrated capabilities for fire detection, the DMSP-OLS is unique in its capability to detect power outages. No other known sensor has this capability.

Over the next year we expect to complete a global map of stable visible-near infrared emission sources which will be available to the scientific community for the analysis of social, environmental, and energy issues. By combining the map of stable lights with observations from single nights, it will be possible to detect both fires and electric power blackouts worldwide, within the observational constraints noted in Section 3.3. In the longer term, we expect it will be possible to periodically update the global city light map to detect the expansion of urban areas. The DMSP program is expected to continue to operate OLS sensors continuously until the later part of the next decade and perhaps until the year 2010. The NOAA-DoD converged

system of meteorological sensors will preserve the low light sensing capability initiated with the OLS. Thus the mapping of stable visible-near infrared emission sources using nighttime satellite data can be expected to be a continuing source of information for the coming decades.

## ACKNOWLEDGMENTS

The authors appreciate the DMSP program office and the U.S. Air Force Global Weather Central for providing NOAA-NGDC with DMSP data used in this research.

## REFERENCES

- Cahoon, D.R., Jr., B.J. Stocks, J.S. Levine, W.S. Cofer, III, and K.P. O'Neill. Seasonal distribution of African savanna fires. *Nature*, 359, 812-815, 1992.
- Croft, T.A. Burning waste gas in oil fields. *Nature*, 245, 375-376, 1973.
- Croft, T.A. Nighttime images of the earth from space. *Scientific American*, 239, 68-79, 1978.
- Croft, T.A. The brightness of lights on Earth at night, digitally recorded by DMSP satellite. *Stanford Research Institute Final Report*, prepared for the U.S. Geological Survey, 1979.
- Eidenshink, J.C. and J.L. Faundeen. The 1-km AVHRR global land data set: First stages in implementation. *International Journal of Remote Sensing*, 15, 3443-3462, 1994.
- Elvidge, C.D., H.W. Kroehl, E.A. Kihn, K.E. Baugh, E.R. Davis, and W.M. Hao. Algorithm for the retrieval of fire pixels from DMSP Operational Linescan System. In: *Global Biomass Burning*, J.S. Levine, Ed., MIT Press, 1996, pp. 73-85.
- Elvidge, C.D., K.B. Baugh, E.A. Kihn, H.W. Kroehl, and E.R. Davis. Mapping city lights with nighttime data from the DMSP Operational Linescan System, *Photogrammetric Engineering and Remote Sensing*, 63, 727-734, 1997.
- Foster, J.L. Observations of the Earth using nighttime visible imagery. *International Journal of Remote Sensing*, 4, 785-791, 1983.
- Goode, J.P. The Homolosine projection: A new device for portraying the Earth's surface entire. *Association of American Geographers, Annals*, 115, 119-125, 1925.
- Lieske, R.W. DMSP primary sensor data acquisition. *Proceedings of the International Telemetry Conference*, 17, 1013-1020, 1981.
- Row, L.W., III and D.A. Hastings. *TerrainBase Worldwide Digital Terrain Data*, Documentation Manual and CD-ROM. NOAA National Geophysical Data Center, Boulder, CO, NGDC Publication KGRD 30, 1995.
- Steinwand, D.R. Mapping raster imagery into the interrupted Goode Homolosine Projection. *International Journal of Remote Sensing*, 15, 3463-3472, 1993.
- Sullivan, W.T., III. A 10 km resolution image of the entire night-time Earth based on cloud-free satellite photographs in the 400-1100 nm band. *International Journal of Remote Sensing*, 10, 1-5, 1989.
- Welch, R. Monitoring urban population and energy utilization patterns from satellite data. *Remote Sensing Environ.*, 9, 1-9, 1980.